Image classification and discrimination of COVID pneumonia based on convolutional neural network

Chuan Qin[a,*], Xuesong Liu[a], Yuanxi Che[b], Enjie Yao[c]
[a] School of Computing, Newcastle University, Newcastle Upon Tyne, UK, NE1 7RU; [b]Department of Electronic and Electrical Engineering, The University of Sheffield, Sheffield, UK, S10 2TN; [c]Department of Computer Science and Technology, Northwest University, Xi'an, China, 710127

ABSTRACT

To address the negative quality of RT-PCR and the time taken to obtain results, this paper reports on the classification and discrimination of COVID pneumonia images by developing a neural network adaptively. Given the limited number of published COVID-19 CT data currently available, we suggest using the proposed negative process to refine the data to obtain more CT data to reduce matching risk; Experimental results show that compared to network models such as AlexNet and GoogleNet, the proposed BUF-Net network model has the best performance with an accuracy of 93%. Visualization of systemic findings using Grad-CAM techniques may further elucidate the critical role of CT imaging in the diagnosis of COVID-19.Conclusion: The use of deep learning tools in clinical practice can help radiologists make better diagnoses.

Keywords: Coronavirus; Deep learning; CT image; Conditional generation countermeasure network; U-Net

1. INTRODUCTION

COVID-19 causes fever, cough, shortness of breath, sore throat, headache, diarrhea, and shortness of breath. Currently, the official method for detecting SARS-CoV-2 is nucleic acid detection by reverse transcription polymerase chain reaction (RT-PCR). Because SARS-CoV-2 can be transmitted during the early stages of infection, nucleic acid detection by RT-PCR is necessary for the early diagnosis of asymptomatic patients. Since virus infection generally starts from the nasopharynx, the specimen collection method of COVID-19 nucleic acid detection is mainly nasal swab and pharyngeal swab [1]. However, there are some problems in the way of nucleic acid detection, such as poor sensitivity of reagents, leading to missed diagnosis and misdiagnosis, long detection time, false negative test results, etc. Since SARS-CoV-2 is transmissible early in infection, nucleic acid detection by RT-PCR is necessary for early diagnosis of asymptomatic patients. In order to eliminate this problem, chest CT scanning is generally used as the main auxiliary diagnostic means. "Guidelines for the imaging diagnosis of new coronavirus pneumonia (2020 First Edition)" suggests that CT scanning should be used to examine patients with COVID-19. High resolution CT scanning with raw data is conducive to the observation and display of details of chest lesions (such as interlobular septum and ground glass shadow), which is of great value for auxiliary diagnosis; Chest CT examination is convenient and easy. It is a good screening method for people who have a travel history in high-risk areas, close contacts with confirmed patients and fever patients. Medical staff can stage viral infection according to different characteristics of lung CT images, such as multiple nodules and interstitial changes in the early stage, focal fusion in the advanced stage, unclear boundary, multiple ground glass shadows, interstitial edema and thickening[2].

*hedy-chuan.qin@outlook.com

Seventh International Conference on Mechatronics and Intelligent Robotics (ICMIR 2023), edited by Srikanta Patnaik, Tao Shen, Proc. of SPIE Vol. 12779, 127792L · © 2023 SPIE · 0277-786X · Published under a Creative Commons Attribution CC-BY 3.0 License · doi: 10.1117/12.2689166

With the continuous development of imaging technology and the increasing level of software and hardware, imaging spectrometers can extract more and more spectral band data, and the spectral range has gradually transitioned from visible light to infrared light, and hyperspectral remote sensing has emerged as the times require. Because hyperspectral remote sensing has multiple spectral channels and the continuity between adjacent spectral channels, hyperspectral remote sensing image data contains a variety of spectral information and spatial information. At present, there are mainly the following problems in the classification of hyperspectral images: (1) Since hyperspectral imaging is constantly transitioning from broadband imaging to narrow-band imaging, hyperspectral image data contains many imaging bands with strong correlation, resulting in a large number of redundant imaging. (2) Commonly used unsupervised classification methods are K-nearest neighbor method, ISDOATA, etc. The above methods are highly affected by the value of similarity evaluation, that is, they are very sensitive to external factors such as noise. Control methods include minimum distance classification, maximum likelihood classification, and support vector machine (SVM)-based methods. These methods use prior knowledge of labeled training samples to train the classifier and obtain the classifier parameters. Then use it to classify the unknown class data.

In this paper, we proposed a method to diagnose COVID based on CT images of patients' lungs and used adversarial generative networks to enhance the dataset of deep neural networks to achieve better results. Compared with other classical neural networks, the proposed BUF-Net network model achieves the best performance with an accuracy of 93%.

2. RELATED WORK

Shao, N. applied deep learning technology to recognize the XR image of epidemic and provide critical reading of a large number of statistical results obtained using currently available data sets [3]. Dong, H. applied convolutional neural network Xception combined with transfer learning method to automatically detect XR image recognition epidemic, and achieved better detection results [4]. XX, A. for the detection of epidemic cases in chest XR images, a low complexity deep convolution neural network COVID net is proposed to achieve 93% classification accuracy [5]. Brik, B. proposed the deep convolution neural network model Coronet based on Xception, and used the pre training method based on ImageNet data set to recognize the XR image of epidemic, achieving a classification accuracy of 94.59%[6]. Adler, A. proposed a DarkCOVIDNet model based on Darknet layer, which automatically detects epidemic cases from chest XR images, with only 1.1 million parameters, and an accuracy of 87%[7]. Zhu, H. applied the artificial intelligence method to retrospectively analyze the chest CT image characteristics and clinical data of 52 patients with mild imported epidemic in some areas of Shenzhen. At the same time, two senior imaging professionals independently analyzed and confirmed the results of each image. It was found that compared with the artificial reading, the chest CT image analysis based on artificial intelligence can directly display the distribution characteristics and size of lesions in the form of specific data [8]. Li, X. used the transfer learning method to extract CT image features, recognize epidemic, modify the typical inception network, and use the pre training weight to fine tune the m-inception model. The experimental results show that the deep learning method is very valuable for extracting radiation image features [9]. Li, Z. based on the v-net model, using the bottleneck structure, obtained a lightweight 3D convolutional neural network VB net model, which automatically and quantitatively analyzed the volume and density of the infected area in the CT image of epidemic [10]. Liu, X. proposed a deep learning method based on transfer learning and self supervised learning to recognize CT image data set and detect cov1d-19, achieving 85% F 1 value and 0.94 AUC [11]. Fang, Q. used a government study to analyze 3epidemic from chest XR images and proposed interventions and integrations that allow clinicians to benefit from the rich benefits of personal data while protecting privacy [12]. Alhudhaif, A. Presenting a deep learning model for visual image extraction from chest volume CT images for epidemic detection. 4352 chest tomography of 3322 patients from 6 hospitals were examined. The performance of the model was evaluated in terms of AUC, specificity, and sensitivity, which were 0.95%, 87%, and 92%, respectively [13]. Valencia, C. F. Presenting a deep learning model for diagnosing epidemic from CT images. This model was not initialized with transfer training, and three deep neural network models were initially trained: AlexNet, GoogleNet, and RESNET. The EDL-COVID split was accepted by a majority. An analysis of 2,933 lung CT images of 2,933 patients with epidemic obtained from previous reports, media, and public registries yielded positive results [14]. Philip, B.v. proposed an automatic deep learning method mnas3dnet41 based on CC-CCII large-class CT image datasets for error correction, noise removal, generation of clean and segmented CT data, and testing on 3D and 2D CNN models deep learning models. This method achieved 87.14% accuracy, 87.25% F1 value, and 0.957 AUC [15].

This paper proposes a novel CT image-based multi-layer perceptron network for the diagnosis of epidemic by improving the limited data with the CGAN technique and integrating the rest into the U-Net network.

3. OUR METHOD

3.1 Basic principle of generating countermeasure network

There are two main designs in Generative Adversarial Networks, which are generators to generate close-to-real images and discriminators to separate real and generated images. During Gan training, the generator and the discriminator are trained sequentially[17]. The goal of training the generator is to produce images that can successfully fool the discriminator. There is no ultimate winner in the game between generators and discriminators. GAN training is expected to find a Nash equilibrium between the generator and the discriminator. The discriminator is no longer able to successfully determine whether the image came from the creator and can only guess at random results. At this point, the generator assumes that it has learned a distribution that maps the noise from the training data to the real data, and can create images that confuse real and fake.

As shown in Figure 1, G represents the generator network, which is a neural network defined by parameter θ_g, and D represents the discriminator network, which is defined by parameter θ_d. In the original GAN, multilayer perceptron is used to build the network, and since DCGAN, it is mostly convolutional neural network [18]. The input of the generator network is random sampling noise g obeying arbitrary distribution P_z, and the output is the mapping $G(z;\theta_g)$ from pseudo data P_z to real data distribution calculated by θ_g. The input x of the discriminator $D(x;\theta_d)$ is the real image and the generated image, and the output model considers the probability that x is the real image.

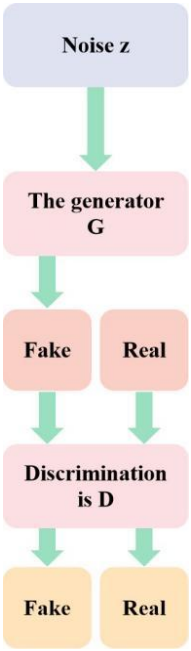

Figure 1. Generation countermeasure network structure

The training of GAN will be a minimax game of two models G and D, and the objective function $V(G,D)$ is shown in formula (1):

$$\min_G \max_D V(G,D) = \mathbb{E}_{x\sim p_{\text{data}}(x)}[\log D(x)] + \mathbb{E}_{z\sim p_z(z)}[\log(1 - D(G(z)))] \quad (1)$$

When training the discriminator, if the input is a real image, $D(x)$ expects the output to be close to 1; If the input is the image generated by the generator, $D(G(z))$ expects the output to be 0, and in general, the objective function is expected to be maximized. When training the generator, the output value of the image generated by the generator after passing through the discriminator is expected to be as close to 1 as possible, that is, $D(G(z))$ is close to 1. At this time, the expected objective function is minimized.

In order to solve the minimum and maximum value problem of objective function 1, an iterative method must be used to train Gan, and the optimization of generator and discriminator needs to be performed in turn [19]. It can be seen from equation 1 that the gradient of the generator's objective function depends on the effect of the discriminator, so in an iteration, it is necessary to update the parameters of the discriminator first.

For any generator A, the training standard of the discriminator is to maximize $V(A, e)$, expand equation (1) to obtain the following equation (2):

$$\begin{aligned} V(g,e) &= \int_x p_{\text{data}}(x)\log(e(x))dx + \int_z p_z(z)\log(1-e(A(z)))dz \\ &= \int_x p_{\text{data}}(x)\log(e(x)) + p_g(x)\log(1-e(x))dx \end{aligned} \tag{2}$$

Let equation (2) take the derivative of $e(x)$ and let the derivative be 0, and the optimal discriminator is the following equation (3):

$$\mathrm{e}_{\mathrm{A}}^{*}(x) = \frac{p_{\text{data}}(x)}{p_{\text{data}}(x)+p_g(x)} \tag{3}$$

From equation (3), it can be seen that the essence of the discriminator is to distinguish whether sample x comes from real distribution p_{data} or generated distribution p_g. The goal of GAN training is to make $p_g = p_{data}$. From equation (3), we can know that $\mathrm{e}_{\mathrm{A}}^{*}(x) = 1/2$. At this time, the discriminator cannot distinguish which distribution the sample comes from, and can only give a probability of 1/2 for both. Bring the optimal discriminator into equation (1), and the loss function of the generator is the following equation (4):

$$\begin{aligned} \mathcal{L}_{\mathrm{A}} &= \max_{\mathrm{e}} V(A,e) \\ &= \mathbb{E}_{x\sim p_{\text{data}}}\left[\log \mathrm{e}_{\mathrm{A}}^{*}(x)\right] + \mathbb{E}_{x\sim p_g}\left[\log\left(1-\mathrm{e}_{\mathrm{A}}^{*}(x)\right)\right] \\ &= \mathbb{E}_{x\sim p_{\text{data}}}\left[\log\frac{p_{\text{data}}(x)}{p_{\text{data}}(x)+p_g(x)}\right] + \mathbb{E}_{x\sim p_g}\left[\log\frac{p_g(x)}{p_{\text{data}}(x)+p_g(x)}\right] \end{aligned} \tag{4}$$

The following formula (5) can be found:

$$\log 2 + \log\frac{\mathrm{c}}{c+d} = \log 2\frac{\mathrm{c}}{c+d} \tag{5}$$

Therefore, equation (4) can be written as the following equation (6):

$$\begin{aligned} \mathcal{L}_A &= \mathbb{E}_{x\sim p_{\text{data}}}\left[\log\frac{p_{\text{data}}(x)}{p_{\text{data}}(x)+p_g(x)}\right] + \mathbb{E}_{x\sim p_g}\left[\log\frac{p_g(x)}{p_{\text{data}}(x)+p_g(x)}\right] \\ &= \mathbb{E}_{x\sim p_{\text{data}}}\left[\log\frac{p_{\text{data}}(x)}{\frac{1}{2}[p_{\text{data}}(x)+p_g(x)]}\right] + \mathbb{E}_{x\sim p_g}\left[\log\frac{p_g(x)}{\frac{1}{2}[p_{\text{data}}(x)+p_g(x)]}\right] - 2\log 2 \end{aligned} \tag{6}$$

Here we introduce two commonly used statistical methods to measure the similarity between probability distributions Y and U: KL divergence and JS divergence. Their definitions are as follows (7) (8):

$$KL(Y \parallel U) = \mathbb{E}_{x\sim P}\log\frac{Y}{U} \tag{7}$$

$$JS(Y \parallel U) = \frac{1}{2}KL\left(Y \parallel \frac{Y+U}{2}\right) + \frac{1}{2}KL\left(U \parallel \frac{Y+U}{2}\right) \tag{8}$$

According to equations (8) and (9), equation (6) can be further deformed into the following equation (9):

$$\mathcal{L}_{\mathrm{A}} = 2JS\left(p_{\text{data}} \,||\, p_g\right) - 2\log 2 \tag{9}$$

Since the divergence between the can be obtained when the two distributions are exactly the same. Therefore, the minimum value of the loss function of the generator is − 2 log 2, if and only if $p_g = p_{data}$. In addition, it can be seen

that when the optimal discriminator has been obtained, the goal of the optimization generator is to reduce the JS between $p_g$and p_{data} [20].

3.2 Condition generation countermeasure network

CGAN consists of two different types of networks: generator networks and discriminant networks. Its structure is shown in Figure 2. Current feedback network models can learn only one type of data at a time, and multi-class batch models must learn in layers. Therefore, the model has the disadvantage of low performance, while the CGAN model adds the same condition to the generator and the discriminator, so GAN can generate different information [21]. The generator used in this paper has 6 transpose convolution layers, 5 ReLU layers, 5 sets of normalization layers, and a Tanh layer at the end. The discriminant network consists of 6 convolutional layers, 5 leaky ReLUs and 4 sets of normalization. Compared with traditional GAN, CGAN adjusts its total loss as Equation (10).

$$\min_{A}\max_{e} V(e,A) = \min_{A}\max_{e}\left(\mathbb{E}_{x\sim p_{\text{data}}(x)}(\ln e(x|Y)) + \mathbb{E}_{z\sim p_z(z)}(\ln(1-e(z|Y)))\right) \tag{10}$$

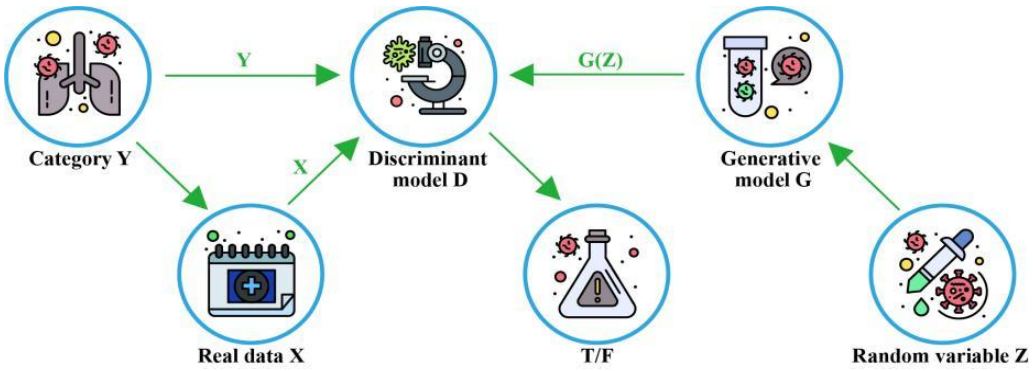

Figure 2. Condition generation countermeasure network structure

3.3 Improved U-Net network structure design

The improved U-Net is a network structure obtained by minor structural adjustment on the basis of u-net. In general, it still adopts a symmetrical encoding and decoding structure and uses jump connection [22]. The model input is the preprocessed 512x512 lung CT image, and the number of channels is 1. The left side of the Figure is the encoder structure. First, the operation flow of "3x3 conv + ReLU", that is, "3x3 convolution layer + correction linear unit" is performed twice continuously on the input data [23]. Then execute the downsampling process for four times, of which the mode of the first three downsampling is the same. First, execute a 2x2 Max pooling operation with a sliding step of 2, and then execute the "3x3 conv + ReLU" operation flow twice in succession. It should be noted that the filling mode of 3x3 convolution layer adopts the same mode, which means that 0 will be used to fill the edge in the convolution process to ensure that the size of the characteristic image will not change, so the size of the characteristic image before and after convolution is unchanged. After each down sampling, the number of feature channels will increase by 16, and the size of the feature map will be reduced to half of the original. The initial number of channels set in the improved U-Net is 16.

In this paper, a BN layer and a layer with the same number of channels are simultaneously added to a two-layer residual block network, and all BN channels are replaced by residual waste blocks. Hence the original design. The remaining parts simultaneously provide layer and BN layer properties. First, the convergence speed of the model increases, and the model does not rely on a good parameter initialization process; Second, we can choose a larger study area to solve the gradient diffusion problem in the backpropagation process; In addition, the frequency of using the release process will decrease, and the capacity of this model will increase to some extent. Figure 3 shows the residual block structure based on the BN layer, and Figure 4 shows the residual block structure based on the BIN layer. The core layer consists of a 32-channel BN layer and a 32-channel inner layer. Adding a BN layer and an inner layer can not only speed up the loss but also preserve the semantic information of the training features [24].

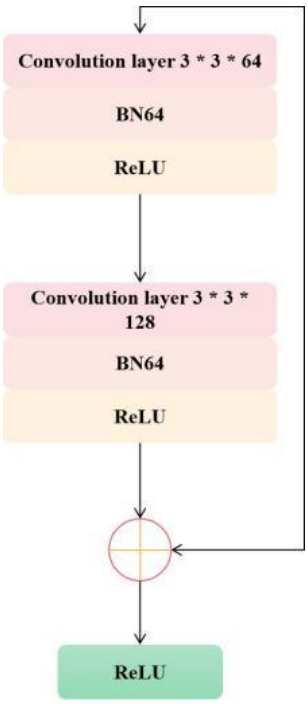

Figure 3. Residual block structure BN layer

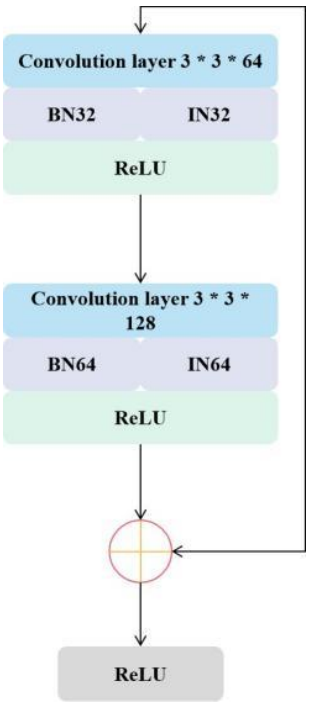

Figure 4. Residual block structure BIN layer

3.4 Model of this paper

The algorithm used in this paper is divided into three steps: (1) Preprocessing. First, the collection of epidemic CT data is usually pre-processed by rotation, rotation, offset, scaling, etc. After that, the data set is leveled using improved connectivity testing. number of samples [25]. (2) Train the model. To reduce the spatial dimension, transform and merge operations are alternately used at the encoder to modify all the connection layers in the encoding layer and the decoding layer to better extract the hierarchical features. Both 3x3 rotation, 3x3 bin residue block, and 2x2 merge operations are used. Performs a rotation function to achieve image pre-removal. The remaining block adds the input to the result of two layers that effectively reduce the gradient loss. The purpose of using business integration is to reduce and prevent conflicts. The decoder part is symmetric with the encoder part and has two 3x3 rotations and one 3x3 in the residual block to recover the spatial dimension and lost content of the target object caused by the fusion operation. Finally, add a 1x1 rotation layer to the final category. Deconvolution can halve the number of channels and double the image quality resolution. The output of the improved U-Net network is a 32x32x1024 tensor. Finally, to perform the classification, the data is transformed into a tensor match with a smoothing function. Multilayer Perceptron (MLP) consists of two layers of 128 and 64 neurons, and the processing unit is ReLU. Finally, image classification is performed using the sigmoid layer thickness activation function and a single neuron. The network model was able to correctly classify CT images in an average of 1.79 seconds. (3) Performance Evaluation: The strengths and weaknesses of the application process will be evaluated using evaluation criteria.

4. EXPERIMENTAL RESULTS

4.1 Materials

The ability to generate negative bias networks is used in data processing to increase the number of samples in the data set and reduce the probability of better results. Table 1 shows the distribution of the data[16].

Table 1. Dataset distribution of CT images

	Train set		Validation set		Test set	
Dataset	COVID-19	NonCOVID-19	COVID-19	NonCOVID-19	COVID-19	NonCOVID-19
COVID19	244	278	71	80	34	39
COVID19+	1 466	1 667	419	476	209	239

4.2 Experimental design

4.2.1 Experimental environment

This test is used for Windows 10 operating system. This is ensured by creating and running deep learning activities using the keras library in the TensorFlow backend, supported by the cuda10.0 and cudnn8 acceleration packages.

4.2.2 Experimental setup

The initial training value and power were set to 0.001 and 0.9 in the training model. In addition, early detection techniques can be used to prevent the network from collapsing, i.e., training can be stopped before a consistent result has reached the truth. Set it to 40 and train the model 100 times. Model hyperparameters optimized by stochastic grid search: (1) momentum; (2) SGD optimizer initial training cost.

4.2.3 Evaluation index

Five different evaluation methods, including accuracy, precision, sensitivity, F1 score, and specificity, were used to evaluate the process of diagnosing epidemic based on CT images proposed in this paper. Among them, accuracy refers to the percentage of correctly identified samples for each sample. As shown in formula (11); The truth is expressed by the formula (12), Represents the ratio of the number of identified samples to the total number of sequences to be analyzed; As shown in Equation (13), the sensitivity, i.e., the recovery rate, is used to measure the sample recognition; There can be both sensitivity and accuracy. derived from the confusion matrix. The F1 score is a combined assessment of precision and sensitivity as shown in Equation (14); Exceptions refer to the proportion of each negation word as shown in Equation (15); AUC stands for "area under the ROC curve". Compared to ACC, AUC is less sensitive to group differences.

$$\text{Accuracy} = \frac{SD+QW}{SD+QW+LM+CV} \tag{11}$$

$$\text{Precision} = \frac{SD}{SD+LM} \tag{12}$$

$$\text{Sensitivity} = \frac{SD}{SD+CV} \tag{13}$$

$$F1-\ \text{score} = 2 \times \frac{\text{precision} \times \text{sensitivity}}{\text{precision} + \text{sensitivity}} \tag{14}$$

$$\text{Specificity} = \frac{SD}{LM+QW} \tag{15}$$

Among them, SD is the number of correctly classified positive examples, QW is the number of correctly classified positive examples to negative examples, LM is the number of incorrectly classified positive examples, and CN is called the false positive rate. Negative samples refer to the number of misclassifications, known as the false negative rate.

4.3 Result analysis

Five-way cross-validation is used to test the performance of the model, and the training data is divided into five parts. Of these five parts, four parts were selected as training methods and the rest as validation methods. This process was repeated five times to train and evaluate the performance of the proposed model in this paper. This paper compares the (BUF-Net) algorithm with several algorithms reported in other literature to learn more about the performance of the proposed model. Table 2 shows the performance indices (sensitivity, precision, F1 value and sensitivity) of each model. It can be seen that the accuracy and precision of the model presented in this paper are 97.1% and 93.1%, respectively,

and the precision value is not very good compared to other models. Additionally, most other models do not use Grad-CAM technology to view distribution results.

Table 2. Comparison between BUF-Net algorithm and other algorithms

Methods	Model	Sen	Acc	Spe	Pre
Dual-sampling attention network	Attention ResNet34+Dual Sampling	86.9	87.5	90.1	
Adaptive feature selection guided deep forest	AFS-DF	93.1	91.7	89.9	
deep neural networks	DarkCOVIDNet	85.3	87	— —	89.9
tailored deep convolutional neural network	COVID-Net	91	93.3		98.9
machine learning methods	GLSZM-LSTM	97.5	98.7	99.6	99.6
ours	BUF-Net	87.6	93.1	77.3	97.1

A comparison of the confusion matrix between the original dataset a and dataset B after data refinement is shown in Figure 5 and Figure 6 .Figure 7 and Figure 8 show the convergence comparison between the multilayer perceptron model using the improved convolutional. Compared to before the addition of residual blocks, the integration speed improved from round 4 to round 18, and the integration speed remained unchanged after iteration until round 26. Figures 9 and 10 show the comparison between the original data and the improved data design and other classical methods. The results show that AlexNet version 1 has the highest rate of 87.9%. This metric refers to the ability to accurately identify epidemic CT. GoogleNet has good functionality and adds a little extra after data processing. Compared to the pre-development data, the accuracy of VGGNet16 is very good. In this paper, the proposed model is improved on four parameters: precision, accuracy, sensitivity, and F1 index. From all the test results, it can be concluded that the BUF-Net model outperforms other algorithms. After data refinement, the performance is improved and the accuracy rate reaches 93%, which is 9% better than CGAN data refinement. Therefore, it can be concluded that the case for the network has the advantage of improving information. Figure 11 shows the ROC curve of the algorithm proposed in this paper. The AUC value of BUF-Net reaches 0.932. Figure 12 shows the comparison curves of accuracy and loss during training. Use an early stop strategy for loop 40 to prevent instability. As shown in the figure, the accuracy and loss rate of 30 methods are achieved and the loss is reduced by 1.3. No change until 0.13.

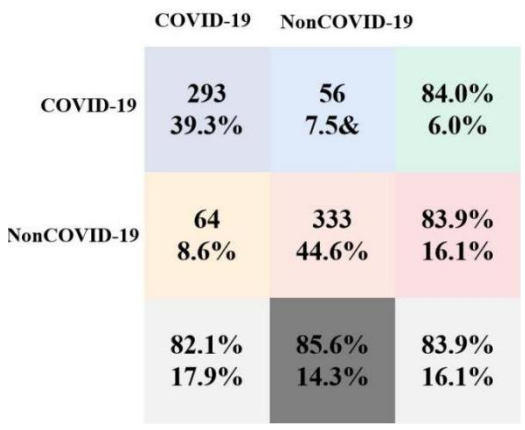

Figure 5. COVID19 confusion matrix

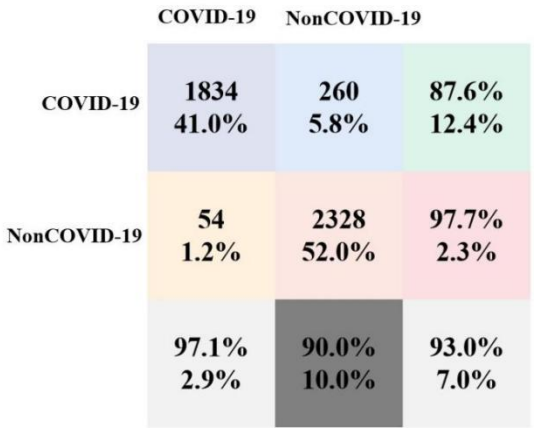

Figure 6. COVID19+ confusion matrix

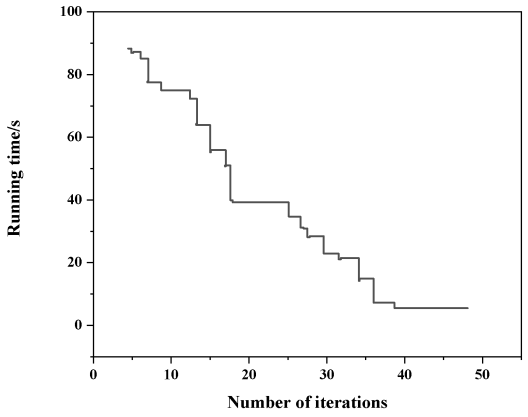

Figure 7. Comparison of U-Net convergence

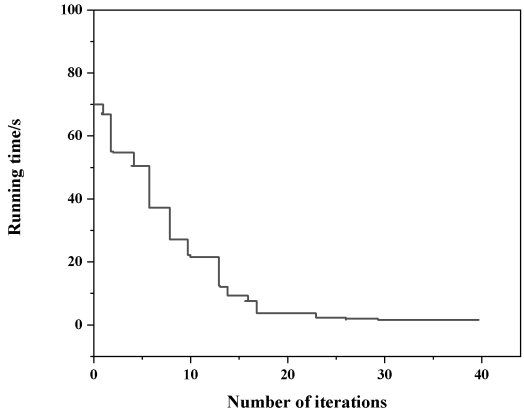

Figure 8. Comparison of U-Net+bin convergence

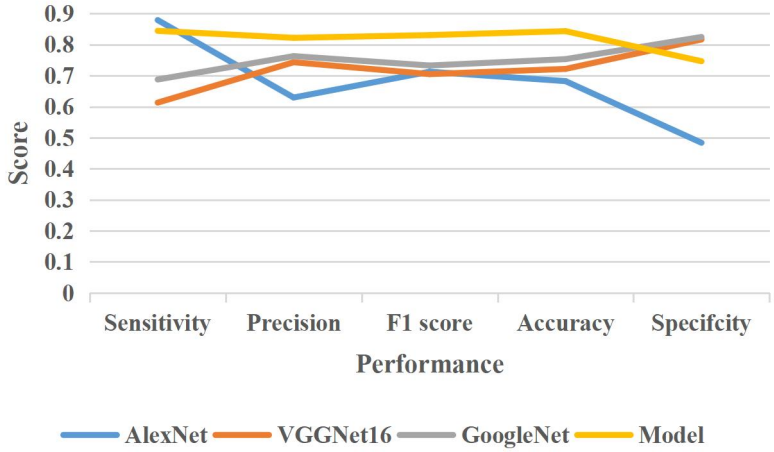

Figure 9. Performance comparison of COVID19

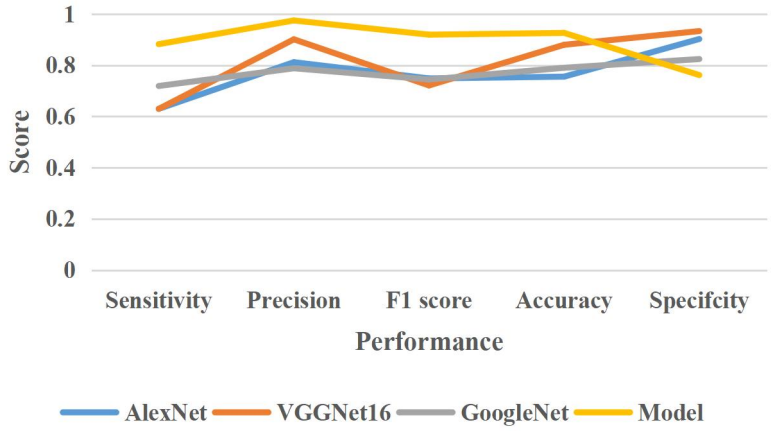

Figure 10. COVID19+ performance comparison

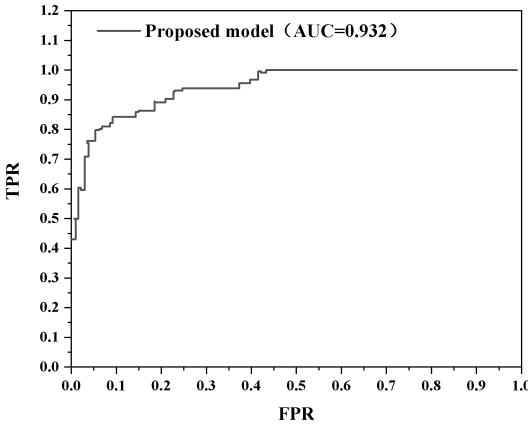

Figure 11. ROC curve of BUF-Net

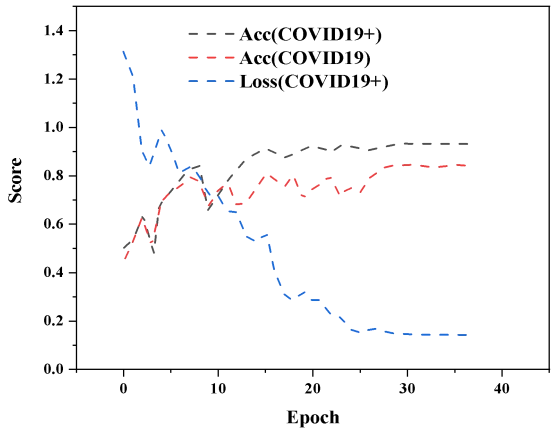

Figure 12. Model training curve of BUF-Net

In this way, the gradient of the class is calculated based on the features extracted from the deepest convolutional layer in the training model, and global averaged into the aggregation layer of the important weights involved in the decision. According to Grad-CAM, it is clear that the proposed model has a good role in the diagnosis of epidemic CT.

5. CONCLUSION

In this paper, we propose a novel dataset enhancement method through conditional generative adversarial networks to reduce the risk of overfitting with small samples of original data; In addition, enhanced CT image data sets are fed into the U-Net network. Combined with multilayer perceptron for clinical segmentation followed by binary classification. Compared with the experimental results of other network models, it shows that it is a good information processing method.

The results of this study show that deep learning can improve diagnosis and improve treatment compared to traditional methods. Although the development of splitting and merging arrangements in this paper can improve the accuracy, there are still some shortcomings. The sample size of the data set in this study is still small, and the results are easy to adjust. Therefore, in future work, I should consider using a deep data model. In addition, we need to find more information about the development process to test the effectiveness of the research methods described in this paper.

REFERENCE

[1] Taresh, M. M., Zhu, N., Ali, T., Hameed, A. S., Mutar, M. L., Transfer learning to detect COVID-19 automatically from x-ray images using convolutional neural networks. International Journal of Biomedical Imaging, (1):1-9 (2021).

[2] Hunter, L., Buchanan, S. A., Responsive stewardship and library advocacy in dystopian times: using information from the civil rights movement and 1984 to strengthen libraries. Online Information Review, 45(4): 853-860 (2021).

[3] Shao, N., Zhong, M., Yan, Y., Pan, H. S., Cheng, J., Chen, W., Dynamic models for coronavirus disease 2019 and data analysis. Mathematical Methods in the Applied Sciences, 43(7):4943-4949 (2020).

[4] Dong, H., Cao, X., The digital divide behind the news spread of novel coronavirus. Procedia Computer Science, 183(20):820-826 (2021).

[5] Xu, X., Jiang, X., Ma, C., Du, P., Li, X., Lv, S., et al., A deep learning system to screen novel coronavirus disease 2019 pneumonia. Engineering, 6(10), 1122-1129 (2020).

[6] Brik, B., Ksentini, A., Toward optimal mec resource dimensioning for a vehicle collision avoidance system: a deep learning approach. IEEE Network, 35(3), 74-80 (2021).
[7] Adler, A., Araya-Polo, M., Poggio, T., Deep learning for seismic inverse problems: toward the acceleration of geophysical analysis workflows. IEEE Signal Processing Magazine, 38(2), 89-119 (2021).
[8] Zhu, H., Han, G., Peng, Y., Zhang, W., Zhao, H., Functional-realistic ct image super-resolution for early-stage pulmonary nodule detection. Future Generation Computer Systems, 115(1), 475-485 (2021).
[9] Li, X., Feng, G., Zhu, J., An algorithm of l 1 -norm and l 0 -norm regularization algorithm for ct image reconstruction from limited projection. International Journal of Biomedical Imaging, (1), 1-6 (2020).
[10] Li, Z., Zhang, J., Liu, D., Du, J., Ct image-guided electrical impedance tomography for medical imaging. IEEE Transactions on Medical Imaging, 39(6), 1822-1832 (2020).
[11] Liu, X., Zhang, Y., Jing, H., Wang, L., Zhao, S., Ore image segmentation method using U-Net and res_unet convolutional networks. RSC Advances, 10(16), 9396-9406 (2020).
[12] Fang, Q., Tan, Z., Li, H., Shen, S., Wen, S., In-situ capture of melt pool signature in selective laser melting using u-net-based convolutional neural network. Journal of Manufacturing Processes, 68(4), 347-355 (2021).
[13] Alhudhaif, A., Polat, K., Karaman, O., Determination of COVID-19 pneumonia based on generalized convolutional neural network model from chest x-ray images. Expert Systems with Applications, 180(10223), 115141 (2021).
[14] Valencia, C. F., Lucero, O. D., Castro, O. C., Sanko, A. A., Olejua, P. A., Comparison of rox and hacor scales to predict high-flow nasal cannula failure in patients with SARS-CoV-2 pneumonia. Scientific Reports, 11(1), 1-7 (2021).
[15] Philip, B. V., Philip, B. V., Impact of COVID-19 on transgender persons: the need for an inclusive approach. International Journal of Sexual Health, 33(3), 248-267 (2021).
[16] Torres-Macho, J., Sánchez-Fernández, M., Arnanz-González, I., Tung-Chen, Y., Franco-Moreno, A. I., Duffort-Falcó, M., et al., Prediction accuracy of serial lung ultrasound in COVID-19 hospitalized patients (Pred-echovid study). Journal of Clinical Medicine, 10(21), 4818 (2021).
[17] da Silva, A. C., Ribeiro, L. P., Vidal, R. M., Matos, W. O., Lopes, G. S., A fast and low-cost approach to quality control of alcohol-based hand sanitizer using a portable near infrared spectrometer and chemometrics. Journal of Near Infrared Spectroscopy, 29(3), 119-127 (2021).
[18] Mary, M. F., Yogaraman, D., Neural network based weeding robot for crop and weed discrimination. In Journal of Physics: Conference Series (Vol. 1979, No. 1, p. 012027). IOP Publishing (2021).
[19] Chen, W., Yao, M., Zhu, Z., Sun, Y., Han, X., The application research of ai image recognition and processing technology in the early diagnosis of the COVID-19. BMC Medical Imaging, 22(1), 1-10 (2022).
[20] Elpeltagy, M., Sallam, H., Automatic prediction of COVID19 from chest images using modified resnet50. Multimedia Tools and Applications, 80(17), 26451-26463 (2021).
[21] Dogra, J., Jain, S., Sharma, A., Kumar, R., Sood, M., Brain Tumor Detection from MR Images Employing Fuzzy Graph Cut Technique. Recent Advances in Computer Science and Communications, 13(3), 362-369 (2020).
[22] Ajay, P., Nagaraj, B., Jaya, J., Bi-level energy optimization model in smart integrated engineering systems using WSN. Energy Reports, 8, 2490-2495 (2022).
[23] Zhao, X. L., Liu, X., Liu, J., Chen, J., Fu, S., Zhong, F., The effect of ionization energy and hydrogen weight fraction on the non-thermal plasma vocs removal efficiency. Journal of Physics D Applied Physics, 52(14), 145201 (2019).
[24] Huang, R., Yang, X., The application of TiO2 and noble metal nanomaterials in tele materials. Journal of Ceramic Processing Research, 23(2), 213-220 (2022).
[25] Zhan, X., Mu, Z., Kumar, R., Shabaz, M., Research on speed sensor fusion of urban rail transit train speed ranging based on deep learning. Nonlinear Engineering, 10(1), 363-373 (2021).